Supplemental information

Shared GABA transmission pathology in dopamine

agonist- and antagonist-induced dyskinesia

Yoshifumi Abe, Sho Yagishita, Hiromi Sano, Yuki Sugiura, Masanori Dantsuji, Toru Suzuki, Ayako Mochizuki, Daisuke Yoshimaru, Junichi Hata, Mami Matsumoto, Shu Taira, Hiroyoshi Takeuchi, Hideyuki Okano, Nobuhiko Ohno, Makoto Suematsu, Tomio Inoue, Atsushi Nambu, Masahiko Watanabe, and Kenji F. Tanaka
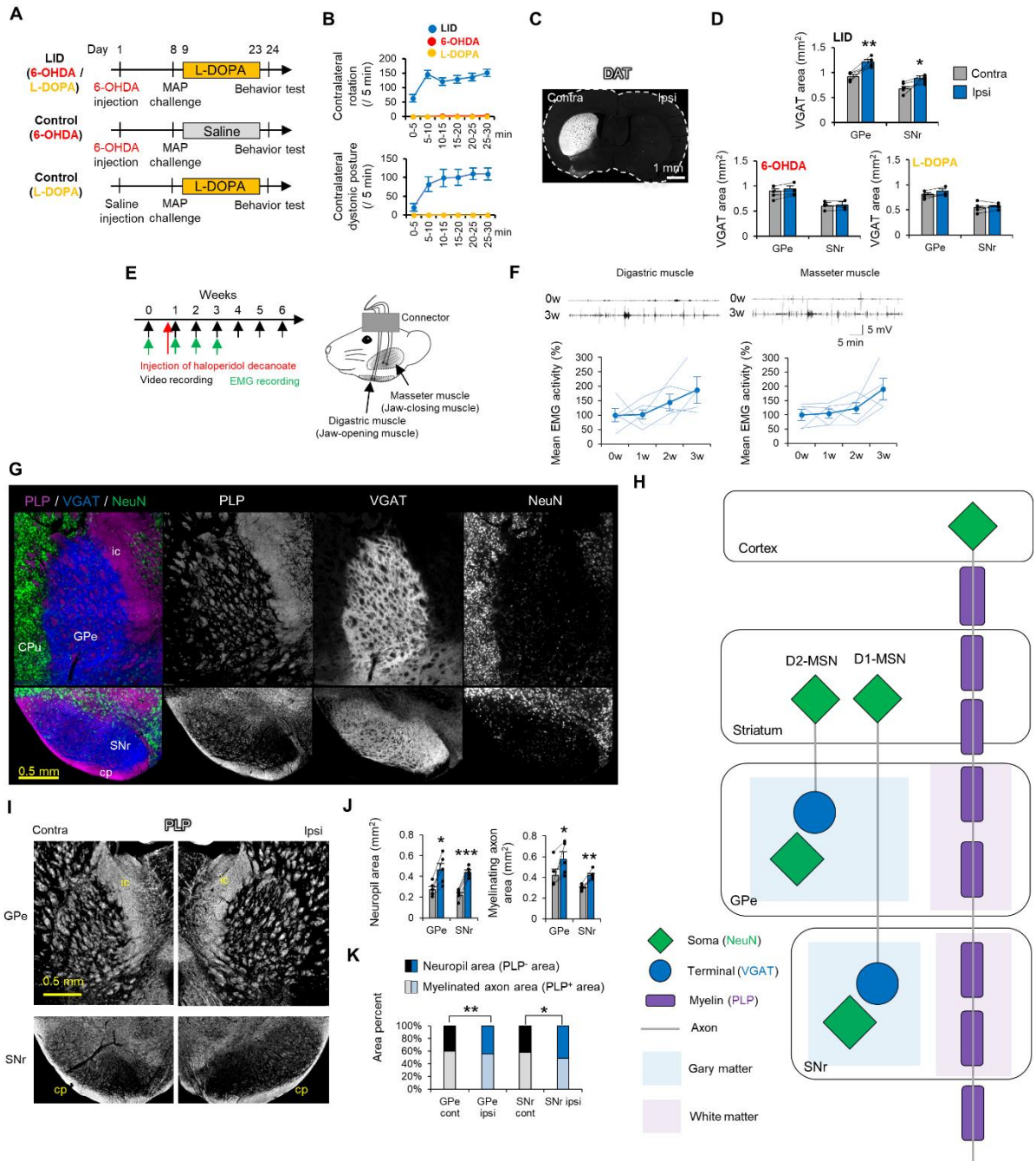
Figure S1. Validation of LID and TD model mice and typical structure of the GPe and SNr, related Figure 1.

(A) Time course of the generation of LID model and control mice.

(B) Number of contralateral rotations and contralateral dystonic postures were counted every 5 minutes in LID model (n=6) and control (n=6) mice.

(C) Dopamine transporter (DAT) staining confirmed dopamine depletion in the Ipsi hemisphere (relative to 6-OHDA injection) compared with the findings in the Contra hemisphere.

(D) VGAT$^+$ area was compared between the Contra and Ipsi hemispheres of LID (n=4) and control (n=4) mice.

(E) Time course of TD model mouse generation. VCMs were recorded by video or EMG every week. EMG was recorded from digastric (jaw-opening) and masseter (jaw-closing) muscles for 3 weeks.

(F) Representative EMG responses from the two muscles at 0 and 3 weeks. Mean EMG activity was plotted every week (n=5).

(G) Representative low-magnification images of PLP, VGAT, and NeuN in the GPe and SNr of control mice. ic; internal capsule, cp; cerebral peduncle. GPe and SNr share a similar structure. They consist of gray matter (VGAT and NeuN) with fragmented white matter bundles (PLP) composed of the myelinated axons of cortical pyramidal neurons.

(H) Schematic diagram of the anatomy of striatopallidal (D2-) and striatonigral (D1-) MSN-terminating nuclei.

(I) Representative images of PLP immunohistochemistry in the Contra and Ipsi GPe and SNr of LID model mice.

(J) The neuropil area (PLP$^-$ area) and myelinated axon area (PLP$^+$ area) were plotted for the GPe and SNr of LID model mice (n=5).

(K) Neuropil and myelinated axon areas were compared between the Contra and Ipsi GPe and SNr in LID model mice (n=5).

*p<0.05. **p<0.01, ***p<0.001 (paired t-test, p-values corrected by Bonferroni correction). Values are plotted as the mean ± SEM.
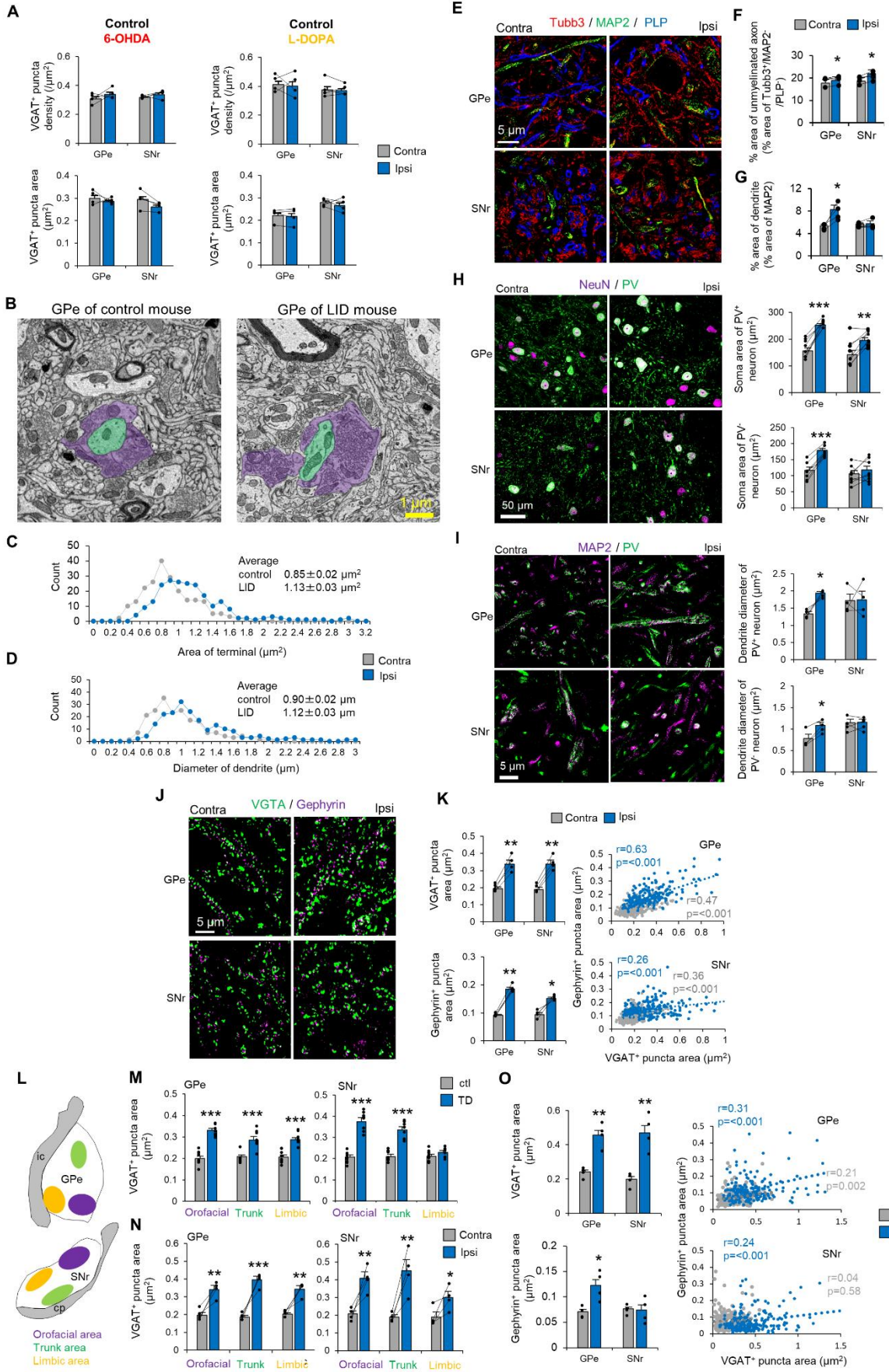
A

Control / 6-OHDA

VGAT⁺ puncta density (/μm²) — GPe, SNr

VGAT⁺ puncta area (μm²) — GPe, SNr

Control / L-DOPA

VGAT⁺ puncta density (/μm²) — GPe, SNr

VGAT⁺ puncta area (μm²) — GPe, SNr

Contra / Ipsi

B

GPe of control mouse   GPe of LID mouse

1 μm

C

Count

Average
control   0.85±0.02 μm²
LID   1.13±0.03 μm²

Area of terminal (μm²)

D

Count

Average
control   0.90±0.02 μm
LID   1.12±0.03 μm

Diameter of dendrite (μm)

Contra / Ipsi

E

Contra   Tubb3 / MAP2 / PLP   Ipsi

GPe

SNr

5 μm

F

Contra / Ipsi

% area of unmyelinated axon (% area of Tubb3⁺/MAP2⁻/PLP⁻) — GPe *, SNr *

G

% area of dendrite (% area of MAP2) — GPe *, SNr

H

Contra   NeuN / PV   Ipsi

GPe

SNr

50 μm

Soma area of PV⁺ neuron (μm²) — GPe ***, SNr **

Soma area of PV⁻ neuron (μm²) — GPe ***, SNr

I

Contra   MAP2 / PV   Ipsi

GPe

SNr

5 μm

Dendrite diameter of PV⁺ neuron (μm²) — GPe *, SNr

Dendrite diameter of PV⁻ neuron (μm²) — GPe *, SNr

J

Contra   VGTA / Gephyrin   Ipsi

GPe

SNr

5 μm

K

Contra / Ipsi

VGAT⁺ puncta area (μm²) — GPe **, SNr **

Gephyrin⁺ puncta area (μm²) — GPe **, SNr *

GPe   r=0.63 p=<0.001   r=0.47 p=<0.001

SNr   r=0.26 p=<0.001   r=0.36 p=<0.001

Gephyrin⁺ puncta area (μm²) vs VGAT⁺ puncta area (μm²)

L

ic   GPe

cp   SNr

Orofacial area
Trunk area
Limbic area

M

GPe   VGAT⁺ puncta area (μm²) — Orofacial ***, Trunk ***, Limbic ***

SNr   Orofacial ***, Trunk ***, Limbic

ctl / TD

N

GPe   VGAT⁺ puncta area (μm²) — Orofacial **, Trunk ***, Limbic **

SNr   Orofacial **, Trunk **, Limbic *

Contra / Ipsi

O

VGAT⁺ puncta area (μm²) — GPe **, SNr **

Gephyrin⁺ puncta area (μm²) — GPe *, SNr

GPe   r=0.31 p=<0.001   r=0.21 p=0.002

SNr   r=0.24 p=<0.001   r=0.04 p=0.58

ctl / TD

Gephyrin⁺ puncta area (μm²) vs VGAT⁺ puncta area (μm²)

Figure S2. The enlargement of inhibitory presynaptic terminal of the MSNs and postsynaptic soma/dendrite of GPe/SNr neurons, related to Figure 1.

(A) The density and area of VGAT$^+$ puncta of MSN terminals were compared between the Contra and Ipsi GPe and SNr in control mice for 6-OHDA (n=4) and L-DOPA (n=4) injections.

(B) Representative EM images of the GPe in control (left panel) and LID (right panel) mice. Green indicates dendrites of GPe neurons and purple indicates MSN terminals.

(C, D) Histograms of the terminal area of MSNs (C) and dendrite diameters (D) of GPe neurons compared between control (n=1) and LID (n=1) mice. For each group, 250 terminals and 200 dendrites were counted from one animal.

(E) Representative SRM images of Tubb3 (myelinated/unmyelinated axons and dendrites), MAP2 (dendrites), and PLP (myelinated axons) immunohistochemistry in LID mice.

(F) Percentage areas of unmyelinated axons (area of Tubb3/area of MAP2 and PLP) in the GPe and SNr were compared between Contra and Ipsi in LID mice (n=4).

(G) The MAP2 area was defined as the area of dendrites of GPe or SNr neurons; percentage areas were compared between Contra and Ipsi hemispheres in LID mice (n=4).

(H) Representative confocal microscopy images of NeuN and PV immunohistochemistry in LID mice. NeuN$^+$ soma areas of PV$^+$ and PV$^-$ neurons were compared between the Contra and ipsi GPe and SNr in LID mice (n=8).

(I) Representative SRM images of MAP2 and PV immunohistochemistry in LID mice. MAP$^+$ dendrite diameters of PV$^+$ and PV$^-$ neurons were compared between the Contra and ipsi GPe and SNr in LID mice (n=4).

(J) Representative SRM images of VGAT and gephyrin immunohistochemistry in LID mice.

(K) Areas of VGAT$^+$ and gephyrin$^+$ puncta of MSN terminals were compared between the Contra and ipsi GPe and SNr in LID mice (n=4). Areas of VGAT$^+$/gephyrin$^+$ puncta in the GPe and SNr in LID mice were plotted. More than 200 puncta were counted from four mice.

(L-N) Three regions of orofacial, trunk, and limbic function were defined in GPe and SNr . Area of VGAT$^+$ puncta of the MSN terminals in three regions of at GPe and SNr were compared between ctl (n=6) and TD (n=6) mice and between the Contra and Ipsi sides of LID mice (n=4).

(O) Areas of VGAT$^+$ and gephyrin$^+$ puncta in the GPe and SNr were compared between control (n=4) and TD (n=4) mice. Areas of VGAT$^+$/gephyrin$^+$ puncta in the GPe and SNr were plotted for control and TD mice. More than 200 puncta were counted from four mice in each group.

*p<0.05, **p<0.01. (Student's or paired t-test, p-values corrected by Bonferroni correction). Values are plotted as the mean ± SEM.
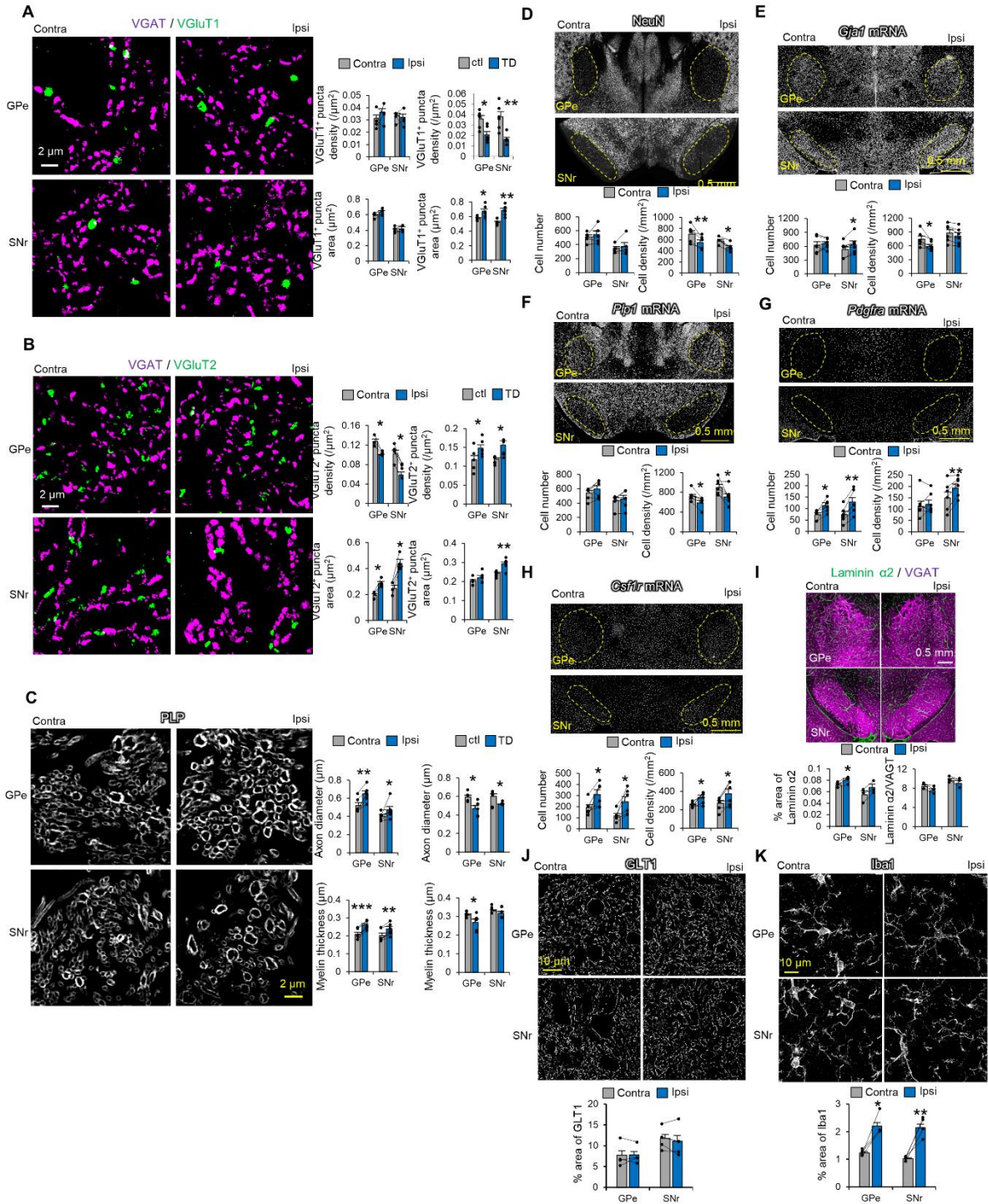
Figure S3. Contribution of another neuronal compartments and glial cells, related to Figure 1.

(A) Representative SRM images of VGAT and VGluT1 immunohistochemistry in LID mice. The density and area of VGluT1$^+$ puncta originating from the cortex were compared between the Contra and Ipsi GPe and SNr in LID mice (n=4). They were compared between TD (n=5) and control (n=5) mice.

(B) Representative SRM images of VGAT and VGluT2 immunohistochemistry in LID mice. The density and area of VGluT2$^+$ puncta originating from the STN were compared between the Contra and Ipsi GPe and SNr in LID mice (n=4). They were compared between TD (n=5) and control (n=5) mice.

(C) Representative SRM images of PLP immunohistochemistry in LID mice. Axon diameter and myelin thickness were compared between the Contra and Ipsi GPe and SNr in LID mice (n=5). They were compared between TD (n=5) and control (n=5) mice.

(D) Representative images of NeuN immunohistochemistry in LID mice. The number and density of NeuN$^+$ neurons were compared between the Contra and Ipsi GPe and SNr in LID mice (n=5).

(E) Representative ISH images of *Gja1* mRNA in LID mice. The number and density of *Gja1*$^+$ astrocytes were compared between the Contra and Ipsi GPe and SNr in LID mice (n=5).

(F) Representative ISH images of *Plp1* mRNA in LID mice. The number and density of *Plp1*$^+$ oligodendrocytes were compared between the Contra and Ipsi GPe and SNr in LID mice (n=5).

(G) Representative ISH images of *Pdgfra* mRNA in LID mice. The number and density of *Pdgfra*$^+$ OPC were compared between the Contra and Ipsi GPe and SNr in LID mice (n=5).

(H) Representative ISH images of *Csfr1r* mRNA in LID mice. The number and density of *Csfr1r*$^+$ microglia were compared between the Contra and Ipsi GPe and SNr in LID mice (n=5).

(I) Representative images of laminin α2 and VGAT immunohistochemistry in LID mice. The percentage area of laminin α2$^+$ blood vessels and normalized laminin α2 area by VGAT area were compared between the Contra and Ipsi GPe and SNr in LID mice (n=3).

(J) Representative SRM images of GLT1 immunohistochemistry in LID mice. The percentage area of GLT1$^+$ astrocytes was compared between the Contra and Ipsi GPe and SNr in LID mice (n=4).

(K) Representative SRM images of Iba1 immunohistochemistry in LID mice. The percentage area of Iba1$^+$ microglia was compared between the Contra and Ipsi GPe and SNr in LID mice (n=4).

*p<0.05. **p<0.01, ***p<0.001 (Student's or paired t-test, p-values corrected by Bonferroni correction). Values are plotted as the mean ± SEM.
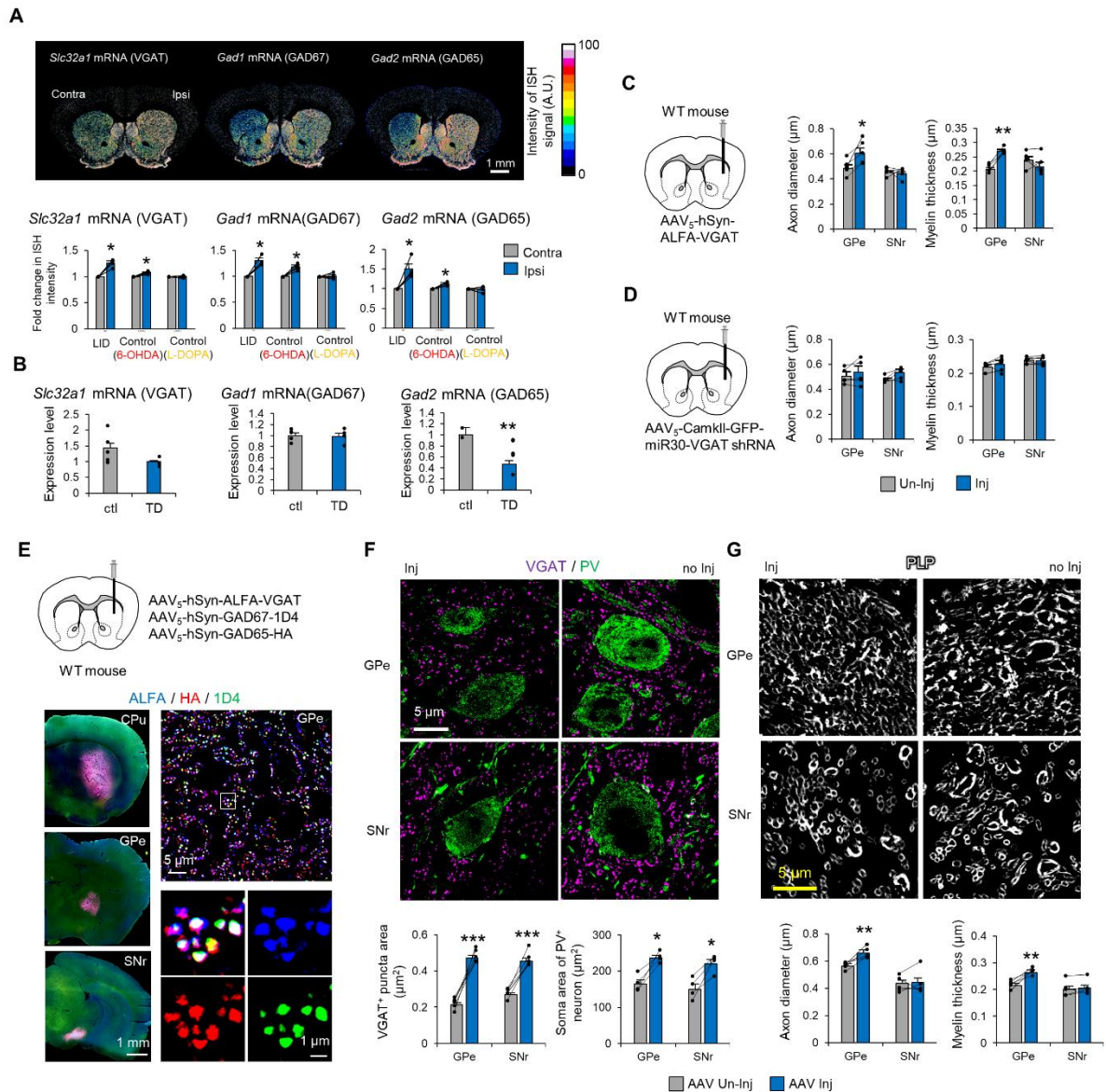
Figure S4. Striatal overexpression of GABA-related genes was associated with dyskinesia-related pathology, related to Figure 2.

(A) ISH images of *Slc32a1*, *Gad1*, and *Gad2* mRNA in LID mice. ISH signal intensities of *Slc32a1* (n=3), *Gad2* (n=4), and *Gad1* (n=4) mRNA compared between the Contra and Ipsi CPu, GPe, and SNr in LID and control mice.

(B) Expression levels of *Slc32a1*, *Gad1*, and *Gad2* mRNA were measured in the striatum of TD (n=5) and control (n=5) mice using quantitative reverse transcription polymerase chain reaction.

(C) AAV vector with ALFA-VGAT was injected into the right dorsal striatum of WT mice. Axon diameters and myelin thickness in the GPe and SNr were compared between the AAV injection (AAV Inj) and non-injection (AAV Un-inj) hemispheres (n=5).

(D) AAV vector with VGAT shRNA was injected into the right dorsal striatum of WT mice. Axon diameters and myelin thickness in the GPe and SNr were compared between the AAV Inj and AAV Un-inj hemispheres (n=5).

(E) A mixture of three AAVs fused with the tag proteins ALFA, 1D4, and HA (ALFA-VGAT, GAD67-1D4, and GAD65-HA) was injected into the right dorsal striatum of WT mice. Representative macroscopic images are of ALFA, HA, and 1D4 immunohistochemistry in the CPu, GPe, and SNr; representative SRM images are from the GPe.

(F) Representative SRM images of VGAT and PV immunohistochemistry in the AAV Inj and AAV Un-Inj hemispheres of WT mice with overexpression. The area of VGAT$^+$ puncta of MSN terminals and the soma area of PV$^+$ neurons in the GPe and SNr were compared between AAV Un-Inj and AAV Inj (n=4).

(G) Representative SRM images of PLP immunohistochemistry in WT mice with overexpression. The axon diameter and myelin thickness of cortical myelinated axons in the GPe and SNr were compared between AAV Un-Inj and AAV Inj (n=4).

*$p<0.05$, **$p<0.01$, ***$p<0.001$ (paired or Student's t-test, p-values corrected by Bonferroni correction). Values are plotted as the mean ± SEM.
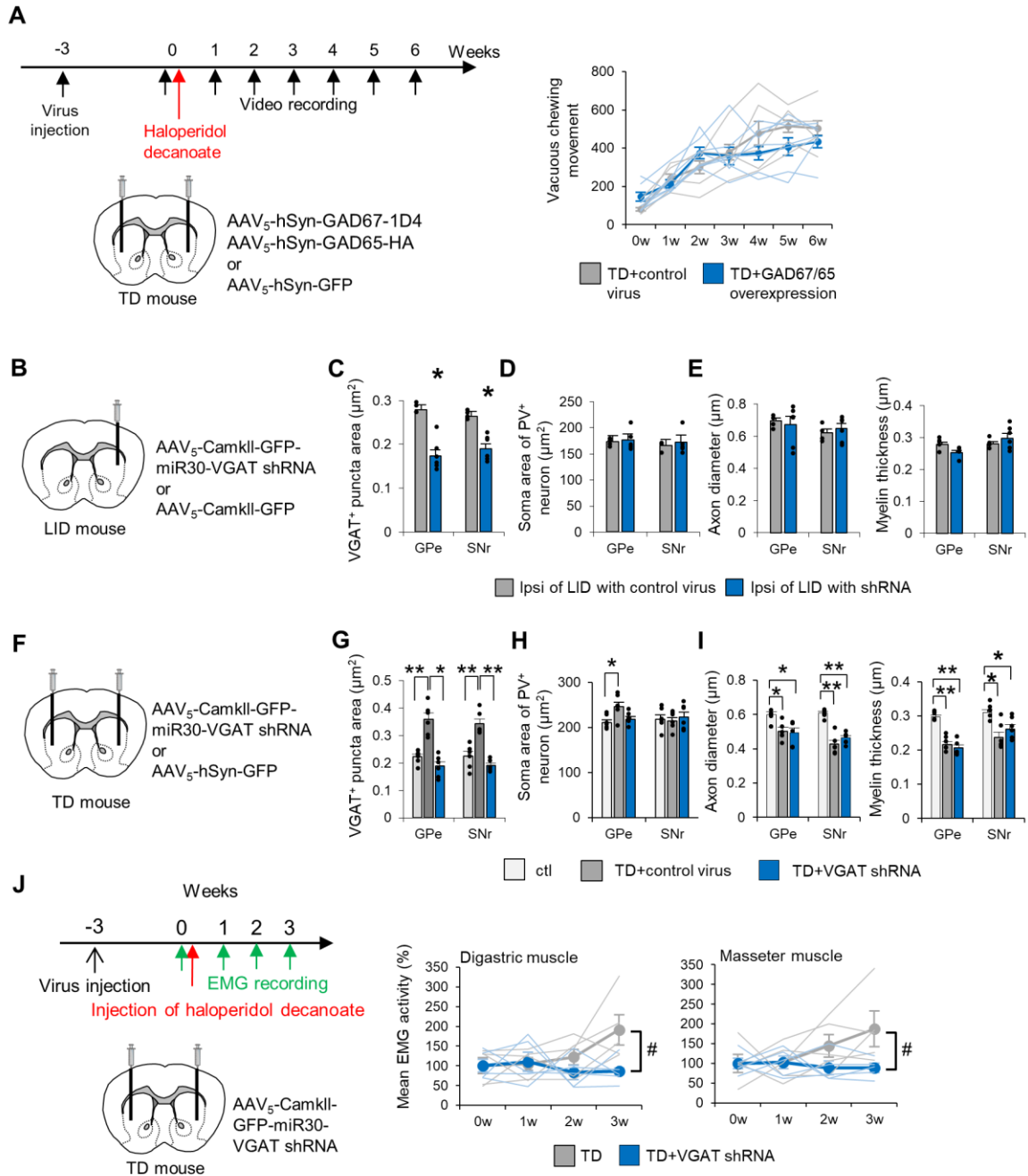
Figure S5. VGAT inhibition suppresses VGAT[+] MSN terminal enlargement but not GPe soma or cortical myelinated axon enlargement, related to Figure 4.

(A) AAV vectors (a mixture of GAD67-1D4 and GAD65-HA, or GFP for the control) were injected into the bilateral dorsal striatum of WT mice 3 weeks before haloperidol decanoate administration. The number of VCMs was compared between TD mice with control AAV (n=6) and TD mice with GAD65/67 overexpression (n=6).

(B) AAV vectors (VGAT shRNA or GFP) were injected into the right dorsal striatum (ipsilateral to the 6-OHDA injection) of LID mice 2 weeks before the 6-OHDA injection.

(C–E) VGAT[+] puncta area of MSN terminals (C), soma area of PV^{+} neurons (D), and axon diameter and myelin thickness of cortical myelinated axons (E) in the Ipsi hemisphere were compared between LID mice with control AAV (n=4) and those with VGAT-shRNA (n=5).

(F) AAV vectors (VGAT shRNA or GFP) were injected into the bilateral dorsal striatum of TD mice 3 weeks before haloperidol decanoate injection.

(G–I) VGAT$^+$ puncta area of MSN terminals (G), soma area of PV$^+$ neurons (H), and axon diameter and myelin thickness of the cortical myelinated axons (I) were compared among control mice (n=6), TD mice with VGAT shRNA (n=6), and TD mice with control AAV (n=6).

(J) AAV vectors (VGAT shRNA) were injected into the bilateral dorsal striatum of TD mice 3 weeks before haloperidol decanoate injection. EMG was recorded from digastric (jaw-opening) and masseter (jaw-closing) muscles for 3 weeks. Mean EMG activity from the digastric and masseter muscles was compared between TD mice with VGAT shRNA (n=5) and TD mice (n=5, same data as Figure S1F).

# $p<0.05$ (two-way repeated ANOVA). *$p<0.05$, **$p<0.01$, ***$p<0.001$ (Student's t-test, p-values corrected by Bonferroni correction). Values are plotted as the mean ± SEM.
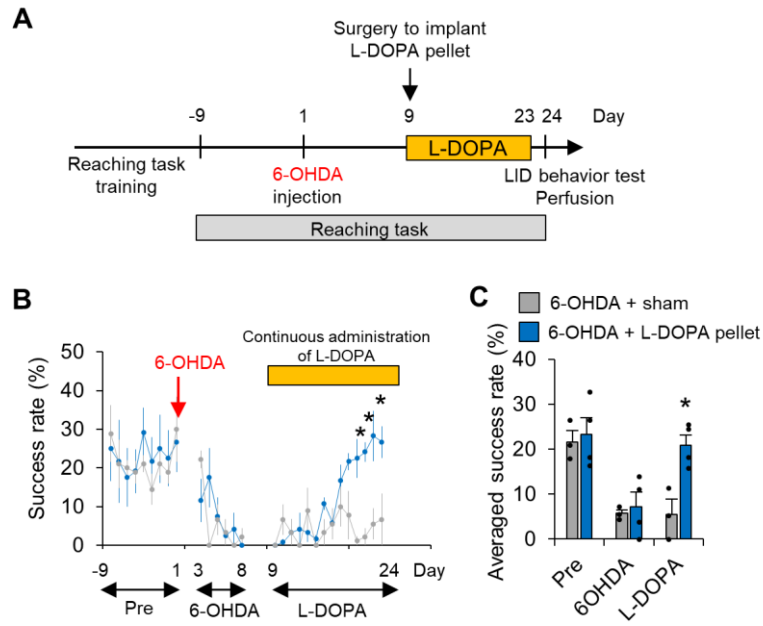
Figure S6. Failure to produce dyskinesia is not the result of insufficient L-DOPA treatment, related to Figure 5.

(A) Experimental time course for the model of continuous L-DOPA administration and reaching task. Mice were trained to perform the reaching task before the 6-OHDA injection, and the L-DOPA pellet was then implanted for continuous administration of L-DOPA. A sham operation was performed in control mice with 6-OHDA. LID behavior was measured after 2 weeks of L-DOPA administration.

(B, C) The success rate (B) and averaged success rate (C) in the reaching task were plotted for three periods: before injection of 6-OHDA (Pre), after injection of 6-OHDA (6OHDA), and after L-DOPA administration (L-DOPA).

*p<0.05 (Student's t-test, p-values corrected by Bonferroni correction). Values are plotted as the mean ± SEM.